Multiple Diffusion Mechanisms Due to Nanostructuring in Crowded Environments

Hugo Sanabria, Yoshihisa Kubota, and M. Neal Waxham
Department of Neurobiology and Anatomy, University of Texas Health Science Center at Houston, Houston, Texas 77030

ABSTRACT One of the key questions regarding intracellular diffusion is how the environment affects molecular mobility. Mostly, intracellular diffusion has been described as hindered, and the physical reasons for this behavior are: immobile barriers, molecular crowding, and binding interactions with immobile or mobile molecules. Using results from multi-photon fluorescence correlation spectroscopy, we describe how immobile barriers and crowding agents affect translational mobility. To study the hindrance produced by immobile barriers, we used sol-gels (silica nanostructures) that consist of a continuous solid phase and aqueous phase in which fluorescently tagged molecules diffuse. In the case of molecular crowding, translational mobility was assessed in increasing concentrations of 500 kDa dextran solutions. Diffusion of fluorescent tracers in both sol-gels and dextran solutions shows clear evidence of anomalous subdiffusion. In addition, data from the autocorrelation function were analyzed using the maximum entropy method as adapted to fluorescence correlation spectroscopy data and compared with the standard model that incorporates anomalous diffusion. The maximum entropy method revealed evidence of different diffusion mechanisms that had not been revealed using the anomalous diffusion model. These mechanisms likely correspond to nanostructuring in crowded environments and to the relative dimensions of the crowding agent with respect to the tracer molecule. Analysis with the maximum entropy method also revealed information about the degree of heterogeneity in the environment as reported by the behavior of diffusive molecules.

INTRODUCTION

Multi-photon fluorescent correlation spectroscopy (MPFCS) (1) is a sensitive and powerful technique for studying biomolecules with single-molecule sensitivity in vitro and, more recently, in the cellular setting. Processes such as aggregation, molecular interactions, binding kinetics, and intracellular diffusion have all been addressed using MPFCS (2). Nevertheless, the complex environment that the intracellular milieu presents to a diffusing molecule makes the interpretation of the experimental results in this setting a complex task. Some possible factors include, but are not limited to: immobile barriers, molecular crowding, and binding interactions.

When discussing diffusion in a complex environment, one could expect to have three qualitatively distinct diffusive behaviors: normal or Fickian diffusion, superdiffusion, and subdiffusion. Typically, these behaviors have been revealed by fitting data to an anomalous diffusion model that introduces a power law function to take into account the environmental variability. When the power exponent α is 1, it corresponds to normal diffusion; superdiffusion and subdiffusion are defined when $\alpha > 1$ and $\alpha < 1$, respectively. We refer to normal diffusion when the mean-square displacement follows a linear function with respect to time with the diffusion coefficient following the Stokes-Einstein equation. The drag force in this relationship is governed by viscosity for the case of an isotropic fluid. However, in a crowded environment, the drag force is generated mainly by collisional interactions between the diffusive molecule and the crowding agent. Superdiffusion is seen when translational mobility has a component of directed motion—for example, when a motor protein ''walks'' on top of a cytoskeleton protein during active transport. This directed motion produces an apparent directional nonrandom flight to the molecules. Other structures can also create superdiffusion, but mainly it corresponds to restricting the mobility to one dimension when other factors are present to direct the diffusive molecule. Subdiffusion occurs when mobility is restricted. Obstacles, structures, or other forces such as inhomogeneous frictional drag present in the environment produce a nonlinear relationship between the mean-square displacement of the tracer molecule and time. A clear example of this nonlinear relationship is when molecules are transiently ''caged'' by the obstacles. All of the previous situations are of particular interest in intracellular diffusion, where molecular crowding, immobile obstacles, and interactions (specific and nonspecific binding) with other molecules affect the range of action of signaling molecules.

In the work presented here, we focus on quantifying the effects of immobile barriers and mobile crowding agents on translational diffusion. We investigate these factors experimentally using silica-based nanostructures to mimic immobile barriers and high molecular mass dextrans as macromolecular crowding agents. We fit these data to the standard form for anomalous diffusion, and also apply the recently developed maximum entropy method for fluorescence correlation spectroscopy (MEMFCS) developed by Sengupta et al. (3). Given distinct differences between the two sets of analyzed data, a discussion of the relative information derived from

Submitted June 5, 2006, and accepted for publication September 26, 2006.

Address reprint requests to Hugo Sanabria, E-mail:hugo.sanabria@uth.tmc.edu.

0006-3495/07/01/313/10 $2.00

doi: 10.1529/biophysj.106.090498

both approaches is presented. The results reveal evidence of various distinct mechanisms, due probably to the formation of ordered structures that are not revealed when analyzing the data by the standard anomalous diffusion model (Eq. 7).

MATERIALS AND METHODS

Preparation of fluorescent molecules

Dextrans-tetramethyrhodamine (dextran-TMR) of 3, 10, 40, and 70 kDa were obtained from Molecular Probes (Eugene, OR; catalogue Nos. D3307, D1816, D1842, and D1819 respectively). Each dextran-TMR was further purified on a HR-12 gel filtration chromatography matrix (Pharmacia, Uppsala, Sweden) using phosphate-buffered saline (PBS); (0.01 M $NaHPO_4$, pH 7.2, 150 mM NaCl) as the running buffer. A single fraction from the peak absorbance at 280 nm of each of the chromatographic runs was used in all of the following experiments. When these fractions were reanalyzed on the same gel filtration column, the peak fit well with a Gaussian distribution (which was not the case with the dextran-TMRs before chromatography).

eGFP-calmodulin (eGFP-CaM) was produced by subcloning the full-length coding sequence of CaM into the eGFP-C2 vector (Clontech, Mountain View, CA). The chimeric eGFP-CaM cDNA was then subcloned into the pFastBac-1 baculovirus expression vector. Recombinant virus and protein were produced in Sf21 cells grown in Excell (Bellevue, WA) 400 defined media as described previously (4). eGFP-CaM was purified from infected Sf21 cell pellets following a protocol for purifying unlabeled CaM as described in detail previously (5). The final protein product was >90% pure when evaluated using SDS-PAGE (data not shown).

Preparation of sol-gels

Sol-gels were formed from silica-based precursors. We used one of the most commonly employed precursors, tetramethoxysilane, or TMOS ($Si(OCH_3)_4$, Sigma-Aldrich, St. Louis, MO). When hydrolyzed in the presence of catalyst, it follows the reaction TMOS + $4(H_2O) \rightarrow Si(OH)_4 + 4\,(CH_3OH)$, liberating methanol as a byproduct. The hydrated silica tetrahedral interacts on a condensation reaction by linking monomers to each other and releasing a water molecule per reaction. A polycondensation reaction follows forming a continuum SiO_2 network that reaches a macroscopic dimension that extends throughout the solution. This process takes place over timescales that are not considered to vary during the data acquisition at each time point. Thus, the aqueous phase consists of a heterogeneous mix of methanol and water. From the initial weight concentration, a molar ratio of 2:1 methanol/water is expected if the amount of water stays constant. However, as the polycondensation occurs, more water molecules are released changing this ratio and therefore altering the viscosity of the aqueous phase in which the molecules diffuse. Polycondensation eventually generates a silica colloid of nanospheres that constitutes the building blocks of the solid skeleton. This silica skeleton enclosing a continuous liquid phase is called sol-gel, whose optical properties are ideal for performing MPFCS. The reaction described above takes place over different timescales. First, the exothermic reaction and formation of the colloidal sol is generated during sonication (6). This is done under an ice water bath for prompt dissipation of thermal energy. Cross-linking of the nanospheres to create an immobile meshwork occurs within the first 6 h under sealed conditions.

The molecules of interest diffuse in the liquid phase that fills the pores. The pore size can be controlled by temperature, water/metal alkoxide ratio, and pH; it can range from a few nanometers to ~100 nm, mimicking size scales relevant to the estimated pore sizes within intracellular spaces. For a comprehensive reference on the physical and chemical properties of sol-gels, we encourage the reader to see Brinker and Scherer (7). Eventually, as the gel ages, molecules become trapped.

Our sol-gel preparation is based on Ellerby et al. (8), where 1 ml of TMOS was hydrolyzed with 227 μl of high-performance liquid chromatography water and 14.7 μl of 0.04M HCl, the latter acting as a catalyst. The mix was sonicated in ice water for 20 min. After sonication, 133 μl of 0.01 M $NaPO_4$, pH 6.0, was added before casting the sol into chambered wells. Fluorescent dextrans tagged with TMR were mixed with the sol to a final concentration of 46 nM. All experiments were performed in eight well chambers mounted on No. 1 glass coverslips that were Parafilm-sealed to avoid evaporation and disturbances from the environment.

Preparation of dextran solutions

High molecular mass dextran solutions (500 kDa; Pharmacosmos A/S, Holbaek, Denmark) ranging from 5% to 30% were made in 1X PBS and were used to create a crowded environment in which fluorescent molecules diffuse. Dextran is a branched polymer polysaccharide linked by 1–6 bonds (9). Most branches contain only one or two monomer units and branching occurs to the extent of 5% (10). Dextran fractions behave as flexible and extended polymers. We made dilutions starting from a 30% dextran and 570 nM of eGFP-CaM solution in 1 X PBS. The solution was sealed and mixed overnight on a magnetic stir plate to ensure homogeneous distribution. A stock of 570 nM of eGFP-CaM in 1X PBS was then added to the already measured solution and diluted to 25% and mixed again. The process was repeated in 5% intervals maintaining the same concentration of eGFP-CaM throughout the titration experiment.

Multi-photon fluorescence correlation spectroscopy

Experimentally, MPFCS (1) was accomplished using the output of a modelocked Ti:S laser (Coherent Mira 900F) pumped by a 5W frequency-doubled Nd:YVO_4 laser (Coherent Verdi-5). A schematic of this set-up is shown in Fig. 1. The intensity was variably attenuated using a filter wheel consisting of metallic neutral density filters. A pair of achromatic lenses (Linos Photonics, Milford, MA) of 20mm and 100mm focal length expanded the beam. The beam was coupled into an inverted microscope (Olympus (Tokyo, Japan) IX-71) through a shortpass dichroic mirror (Chroma (Rockingham, VT) 800dcspxr). An overfilled water-immersion objective lens (Olympus UPlanApo/IR 60X/1.20W) with high numerical aperture (NA) focused the beam onto the sample of interest, which was mounted in a chambered No. 1 coverglass dish (Nalge Nunc (Rochester, NY) 155411). The fluorescence emission was collected by the same objective lens and was transmitted through the shortpass dichroic and a built-in 200 mm focal length (*f*200) tube lens. A detection assembly using an emission filter (Chroma HQ600/200M) was coupled to an XYZ translation mount with an subminiature A fiber connector (AF Optical (Fremont, CA) 20-504). A multi-mode fiber of NA 0.22 with a 105 μm diameter core (Thorlabs (Newton, NJ) AFS105/125Y) was attached at one end to the assembly, and at the other to a photon counting avalanche photodiode (APD) module (PerkinElmer (Wellesley, MA) SPCM-AQR-W4). The TTL pulses produced by the APD was coupled to a commercial autocorrelator board (Correlator.com (Bridgewater, NJ) Flex01-D), which computed a correlation curve from the fluorescence intensity record in real time. The data were collected via a USB using the correlator software, and subsequently analyzed either by custom software developed in MATLAB (The MathWorks, Natick, MA) or using MEMFCS (3) (see below for explanation). Ten recordings of 10 s each were obtained for each sample, unless otherwise specified. Raw data were averaged and the standard deviation was computed for further weighting and error analysis. Measurements were taken at ~6 mW of power at the specimen plane, where photobleaching, focal volume saturation, and heating of the sample are not considered to contribute greatly as determined on this system (11).

Autocorrelation functions

The fluorescence ($F(t)$) emitted by molecules diffusing in and out of the small optically defined focal volume (<1 fL) is recorded via the APD. The

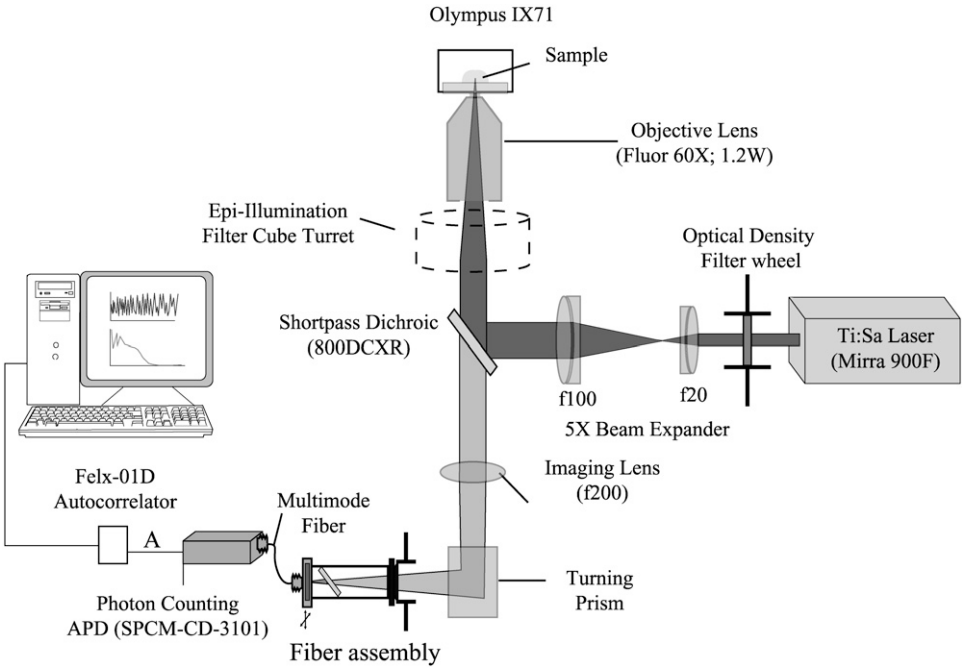

FIGURE 1 Schematic of a two-photon FCS apparatus. The output of a Ti:Sa pulsed laser is expanded into an inverted microscope, where the beam is reflected by a short-pass dichroic mirror and focused by a 60× 1.2 NA water immersion objective into the sample. Fluorescence emission is directed into a custom-built XYZ adjustable multimode fiber assembly. The optical fiber couples the collected photons to an avalanche photo diode, which generates digital signals that are sent to and analyzed in real time on an autocorrelator board before the data are acquired and displayed by the computer.

signal produces fluorescent fluctuations shown as an intensity trace where the mean intensity value is proportional to the average number of molecules present in the volume ($\langle N\rangle$). The autocorrelation function $G(\tau)$ is computed in hardware via the correlator board. Mathematically, this is represented by

$$G(\tau) = \frac{\langle \delta F(t)\delta F(t+\tau)\rangle}{\langle F(t)\rangle^2}, \tag{1}$$

where δF corresponds to deviations from the mean value $\langle F(t)\rangle$. The zero time correlation represents the magnitude of the fluctuation and for a dilute homogeneous solution corresponds to $G(0) = 1/\langle N\rangle$. As $\langle N\rangle$ increases, fluctuations become smaller. Fluctuations in the concentration are defined by the diffusive mechanism of such molecules. Let us consider a single species, which is chemically equilibrated in solution, diffusing in the focal volume described by a three-dimensional Gaussian function. Under these conditions, one can express the autocorrelation function as (12)

$$G(\tau) = \left(\frac{1}{N}\right)\left(\frac{1}{1+\tau/\tau_D}\right)\left(\frac{1}{1+\frac{1}{K^2}\tau/\tau_D}\right)^{1/2}. \tag{2}$$

The structure parameter of the focal volume profile is defined by K and was set to 2.5 for the 60 × 1.2 NA objective used in this study, and τ_D is the characteristic time of the diffusion. τ_D is related to the diffusion coefficient D by

$$\tau_D = \frac{\omega_{xy}^2}{4D}, \tag{3}$$

where ω_{xy} corresponds to the half-width of the detection volume and is specific for the objective used. Other factors have been added to Eq. 2 to describe different behaviors, such as focal volume saturation (13,14) and photobleaching (15–17), which are not considered to be factors at the powers used in the presented experiments, unless otherwise specified.

MEMFCS and Fickian diffusion

The fitting function shown in Eq. 2 describes well the behavior of homogeneous populations of molecules undergoing simple Fickian diffusion. However, when a heterogeneous distribution of species is present, the ability to differentiate them by fitting the autocorrelation with a multicomponent model is restricted by difference in size and molecular brightness between the multiple species (12). In the case of two species, their diffusion times must differ by at least a factor of 1.6 for comparable fluorophores to be reliably resolved (18). In addition, one must assume a priori knowledge of the number of species present to apply the proper model to fit the data. An alternative strategy, recently introduced by Sengupta et al., is based on the maximum entropy method (MEM) (19) to obtain the most probable fit when a variety of species are present. A multi-component form of Eq. 2 is introduced and described by

$$G(\tau) = \sum_{i=1}^{n} a_i\left(\frac{1}{1+\tau/\tau_{D_i}}\right)\left(\frac{1}{1+\frac{1}{K^2}\tau/\tau_{D_i}}\right)^{1/2}, \tag{4}$$

where n is the number of non interacting species each with a characteristic residence time τ_{Di}. The MEM, applied to FCS and called MEMFCS from here on, is based on not only minimizing χ^2 to obtain an optimal fit, but also maximizes an entropic quantity $S = \sum_i p_i \ln p_i$, which is related to each of the amplitudes (a_i) by

$$p_i = \frac{a_i}{\sum_j a_j}. \tag{5}$$

MEMFCS maximizes the entropy S under the constraint C, dictated by χ^2. This problem is solved by defining a quantity Q, such that, $Q = \lambda S - C$, where λ is a Lagrange multiplier. Q is extremized in such a way that λ is dynamically adjusted guiding the program toward subsequent lower values of χ^2 along the path of maximum entropy (K. Garai and S. Maiti, Tata Institute of Fundamental Research, personal communication, 2006) as opposed to the algorithm described by Modos et al. (20). For a more detailed explanation on the algorithm per se, see Skilling and Bryan (17). MEMFCS has been applied to reduce bias in the fitting routines and provides a probabilistic distribution of the τ_{Di}s that best agrees with the data (3). For this multi-component model, one has to consider that $G(0)$, instead of corresponding to the inverse of the number of molecules for one component, now corresponds to the sum of all the amplitudes ($G(0) = \sum_i a_i$). One can then normalize the amplitudes a_i by dividing by $G(0)$; a_i now represents the probability that a species i has a translational residence time τ_{Di}.

Anomalous diffusion

The description given above is for n noninteracting, fluorescently labeled species, where molecules are undergoing Fickian diffusion. Diffusion in heterogeneous environments often cannot be well described by assuming Fickian diffusion and can be better described by a more general (phenomenological) description termed anomalous diffusion. Anomalous diffusion occurs when the mean-square displacement follows a power law in the form of

$$\langle r^2(t)\rangle = 6\Gamma t^{\alpha}, \tag{6}$$

where α encompasses deviations from normal diffusion ($\alpha = 1$). The phenomenon for the case of $\alpha < 1$ has been termed subdiffusion, whereas the case of $\alpha > 1$ is termed superdiffusion. Including the α-exponent in Eq. 2 leads to (21)

$$G(\tau) = \left(\frac{1}{N}\right)\left(\frac{1}{1+(\tau/\tau_{\mathrm{Da}})^{\alpha}}\right)\left(\frac{1}{1+\frac{1}{K^2}(\tau/\tau_{\mathrm{Da}})^{\alpha}}\right)^{1/2}. \tag{7}$$

The residence time now is denoted by τ_{Da} to differentiate it from τ_{D}.

EXPERIMENTAL RESULTS

Diffusion in the presence of immobile barriers

Immobile barriers are one of the possible causes of hindered diffusion in the intracellular environment. These could be envisioned as large molecules, organelles, or cytoskeletal structures that, although they move inside the cells, have negligible mobility when compared to the mobility of the diffusive molecule of interest. Sol-gels were used as a way to create optically transparent immobile nanostructures with pores sizes comparable to the diffusive molecule. FCS measurements were made on different-sized TMR-labeled dextran molecules diffusing as the sol-gel polymerized over hours to days (Figs. 2 and 3).

The decreased translational mobility of 3 kDa dextran labeled with TMR is evident as the sol-gel polymerizes and is indicated by the rightward shift in the autocorrelation curves due to shrinking of the pore size (Fig. 2 *a*). Note also that the mobility of the 3 kDa dextran-TMR is significantly slower at time zero, before polymerization has started, than when free in solution (represented by a *vertical dashed line* in panel *c*). Table 1 summarizes the data as the sol-gel ages. The amplitude distributions obtained from the MEMFCS fitting show a time-dependent decrease in magnitude and peak broadening (panel *c*). By 3 days, the translational mobility had reached a plateau and the experiment was not followed further. The presence of a smaller amplitude diffusive component at $\tau_{\mathrm{Di}} \sim 10^{-1}$ ms in the 0 h trace (observed in Fig. 2 *c*) is addressed in more detail below. A similar time-dependent profile was obtained for the mobility of 10 kDa dextran-TMR added to the sol-gel (Fig. 2 *b*). Again mobility was slowed at time zero relative to the molecule free in solution (*vertical dashed line* in Fig. 2 *d*). At the 6-h time point (Fig. 2 *d*), two distinct peaks become evident in the MEMFCS fit of the data that then resolve to a broader single peak at the 3-day time point. This profile is reminiscent of that obtained with the trace of 3 kDa dextran-TMR at 0 h

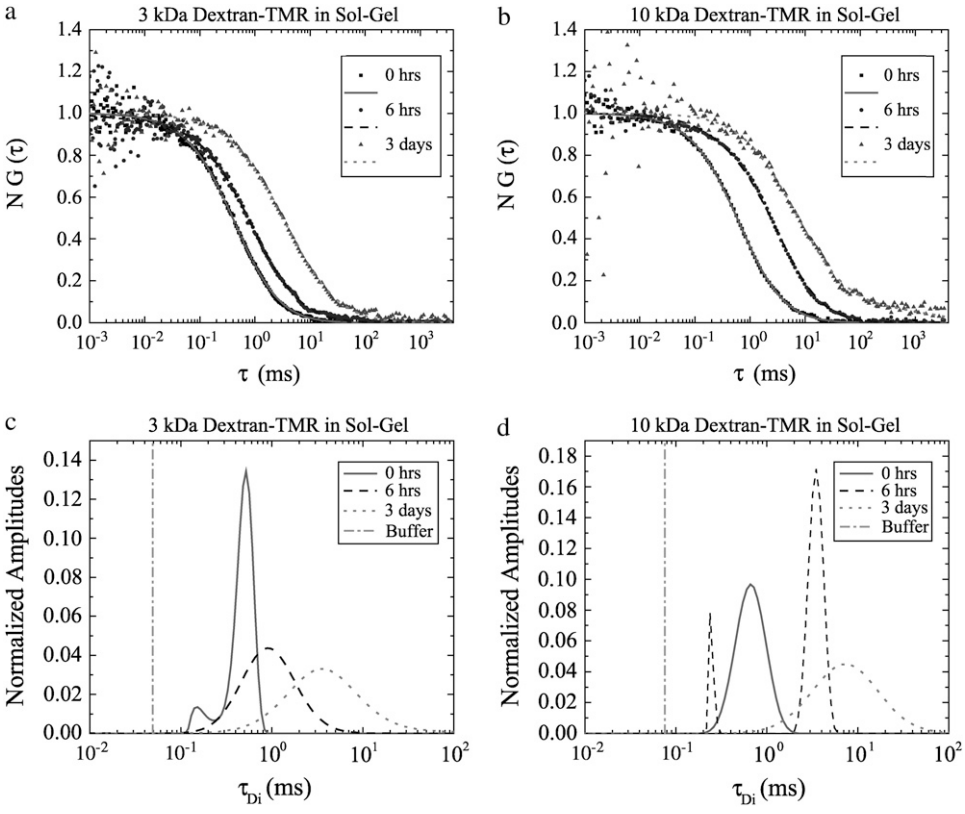

FIGURE 2 FCS for (*a*) 3 kDa and (b) 10 kDa dextran tagged with TMR in sol-gels as polymerization takes place showing a shift toward higher τ values as expected due to the decrease on the pore size. Non-Fickian diffusion is observed as the sol-gel forms and ages over time as observed by the decrease and broadness of the amplitude distributions obtained from MEMFCS fits as shown in panel *c* for a 3 kDa dextran-TMR. At time zero, there is a splitting of the amplitude distribution into two peaks. In panel *d* with 10 kDa dextran, the appearance of two peaks does not appear until the 6 h time point and is explained as the formation of secondary structures that gives a faster diffusing component along with a component representing significantly hindered diffusion. A comparative analysis of the data fit with MEMFCS and an anomalous model is summarized in Table 1. In panels *c* and *d*, a vertical dash line shows the τ_{Dmax} for the diffusive tracer in buffer.

TABLE 1 Change of τ_{DMax} as sol- gels age for different size dextrans tagged with TMR compared to the fitting parameter obtained using the anomalous exponent α

	Time	τ_{DMax} (ms)	τ_a (ms)	α
3kDa dextran-TMR	Free	0.049	0.046	0.95
	0 h	0.52 0.152	0.45	0.96
	6 h	0.90	0.96	0.92
	3 days	3.61	3.68	0.81
10 kDa dextran-TMR	Free	0.076	0.068	0.93
	0 h	0.66	0.66	0.95
	6 h	3.50 0.237	2.59	0.85
	3 days	7.35	9.80	0.74
40 kDa dextran-TMR	Free	0.216	0.200 $\tau_x = 4.88\ \mu s$*	1
	0 h	1.36 0.106	1.15	0.88
70 kDa dextran-TMR	Free	0.230	0.249 $\tau_x = 3.65\ \mu s$*	1
	0 h	1.63	1.64	1

Shown in the first row for each of the different-sized tagged dextran are the characteristic diffusive times obtained using Eq. 4 and Eq. 7 when diffusing ''free''. When two different diffusive mechanisms are observed, the first reported value is the one with highest amplitude and the second one is with the lowest peak amplitude.

*A modified Eq. 2 with a triplet fraction was required to fit correctly these data with a single component model, and τ_x represents the triplet characteristic time.

(Fig. 2 *c*), but now the two peaks are well separated and not adjacent to each other. Table 1 compares the results of fitting the experimental data in Fig. 2 with Eqs. 4 and 7. The anomalous exponent (α) clearly is reduced as the sol-gels age and would be categorized as subdiffusive behavior. Also, τ_{DMax} and τ_a correlate well even though the peaks broaden with time. However, unlike interpretations of pure subdiffusive behavior based on the fits of the data to Eq. 7, the MEMFCS fit of the data extracted evidence for two separate populations of diffusing molecules. A plausible explanation for the two peaks at the 6-h time point is that the 10 kDa dextran-TMR molecules are sensing at least two different environments within the sol-gel matrix. Physically, this would consist of areas of increased obstacle density expected as the sol-gel polymerizes, and also areas where the 10 kDa dextran-TMR can undergo less-hindered diffusion. These could be regions of the sol-gel matrix that exhibit an open volume, or perhaps even areas where the molecules could undergo less-hindered diffusion due to local changes in sol concentration or structures formed inside the solution (see the Discussion section for additional description). It appears that the smaller size of the 3 kDa dextran-TMR molecules make them less sensitive at distinguishing this transition in the sol-gel matrix. Since the 3 kDa and 10 kDa dextran-TMR data were collected under essentially identical experimental conditions, we conclude that it is the size of the fluorescent tracer molecule that dominates the type of diffusive behavior observed.

A unique pattern of diffusive behavior is found when 40 kDa dextran-TMR in sol-gel is measured, as shown in Fig. 3 *a*. Two separate diffusive components can be distinguished by the MEMFCS fitting at time zero indicating that like the 10 kDa dextran-TMR data at 6 h, the 40 kDa dextran-TMR is sensing at least two different physical environments. Interestingly, the population of faster-diffusing 40 kDa dextran-TMR molecules has a peak τ_d that is, within experimental error, close to the τ_d measured for the 40 kDa dextran-TMR in solution. At 1 day, the 40 kDa dextran-TMR exhibits a relatively flat autocorrelation curve that shows an unusual decay at very long τ_Ds and indicates the molecules have become trapped in the shrunken pores of the sol-gel matrix. The decay in the FCS curves at long τ_d is consistent with

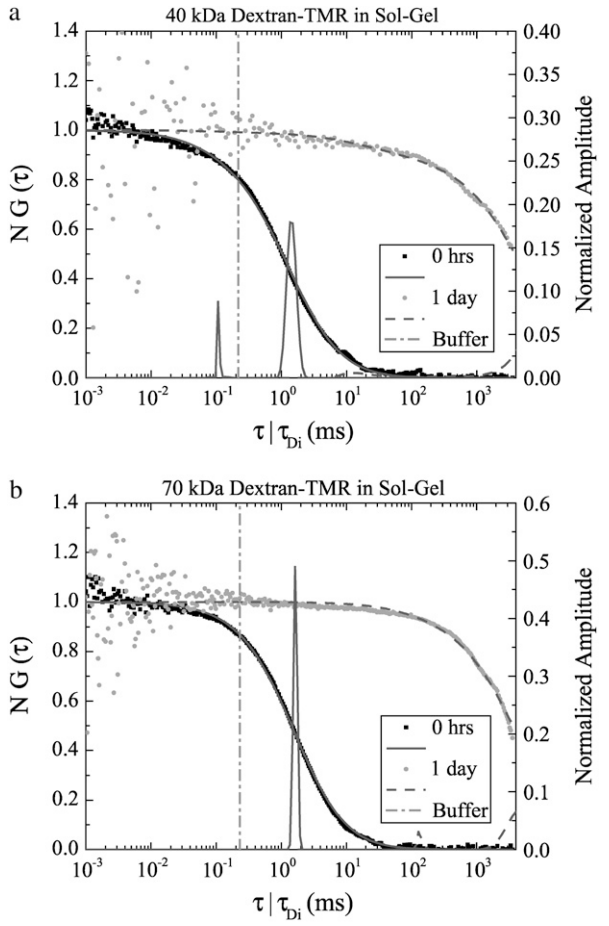

FIGURE 3 FCS and MEMFCS fit for (*a*) 40 kDa and (b) 70 kDa dextran tagged with TMR in sol-gels as polymerization takes place. With the 40 kDa TMR dextran at time zero, two components are revealed as with both the 3 kDa and 10 kDa dextrans (Fig. 2). At 1 day, the pore size is reduced and molecules are trapped. This is observed by a relatively flat autocorrelation curve in green with a very long decay that corresponds most likely to the photobleaching rate of TMR as explained in the text. The fastest peak could be interpreted as molecules observing a less-hindered environment. A similar behavior is seen in panel *b* for 70 kDa dextran, although at time zero, there is only one sharp peak from the amplitude distribution analysis using MEMFCS.

photobleaching of the 40 kDa dextran-TMR immobilized molecule. Results analyzing the diffusion of 70 kDa dextran-TMR in the sol-gel (Fig. 3 *b*) are generally similar to those with the 40 kDa dextran-TMR. One exception is that only one peak was detected when the time zero data were analyzed with the MEMFCS program. This suggests the pores in the sol-gel at time zero present a relatively homogenous profile to the 70 kDa dextran-TMR. Similar to the 40 kDa dextran-TMR at 1 day, the 70 kDa dextran-TMR is trapped and exhibits a flat autocorrelation curve. The drop off in the autocorrelation curve at long τ_ds is nearly identical to the profile seen with the 40 kDa dextran-TMR and supports the idea that this decrease is due to photobleaching of the trapped 70 kDa dextran-TMR. Consistent with the interpretation of photobleaching is that the intensity trace recorded of the raw photon counts (data not shown) decays with a negative slope whose rate correlates with the long τ_d observed in the autocorrelation data.

Table 1 reports the fact that when considering 40 and 70 kDa Dextran-TMR in free solution, data had to be fit with a modified version of Eq. 2 that included a triplet fraction. This was done only because the amount of the triplet fraction was considerably large, probably due to the increased degree of labeling and photophysical characteristics of the TMR dye. However, this is not a significant factor in interpreting the rest of the experiments, since the translational diffusion behaviors are separated by at least two orders of magnitude in timescale. For example, the fastest τ_a obtained for the experiments in sol-gels was ~450 μs compared to the slowest triplet characteristic time τ_x of ~4.88 μs. It is important to note that the amplitude distribution of each of the different tagged dextrans diffusing in buffer shows a sharp distribution normally with three contiguous τ_{Di}s and is centered at τ_{Dmax}. Similar results have been previously reported for different dyes when analyzed with the MEMFCS methodology (3).

An important application in studying diffusive molecules in sol-gels is that FCS can be used with different-sized reporter molecules to provide a quantitative description of the pore size and geometry of sol-gel nanostructures during polymerization. As molecules become trapped and the autocorrelation curve disappears, the pore size would be comparable or slightly below the size of the reporter molecule. Usually the pore size in these materials is determined by gas adsorption and desorption isotherms (22) among others, mostly applied to solids, but currently there are no methods applicable to monitor pore size in the aqueous phase. FCS analysis using a diffusive molecule with known dimensions could serve to locally characterize the physical dimension of the pores.

Diffusion in the presence of molecular crowding

Using FCS, Banks and Fradin (23) recently showed that fluorescently tagged proteins diffusing in a crowded environment show an anomalous type of diffusive behavior. In this report, we used 500 kDa dextran at different concentrations to create a crowded environment and measured the diffusion of eGFP-CaM, our diffusive molecule, using FCS. eGFP-CaM was chosen both from our interests in factors governing the translational mobility of this important cellular signaling molecule and because Fradin and Banks (23) showed that fluorescently labeled dextran molecules did not appear to undergo anomalous diffusion when placed in a crowded dextran environment. The results of such experiments are shown in Fig. 4. When the concentration of 500 kDa dextran is increased, the characteristic time or roll off of the autocorrelation is shifted toward slower timescales as expected, most likely due to the appearance of porosity, or increase in collisions between the tracer and the crowding agent. But the most significant result comes from analyzing the data using MEMFCS. The amplitude distribution was normalized with respect to $G(0)$. At the highest concentration

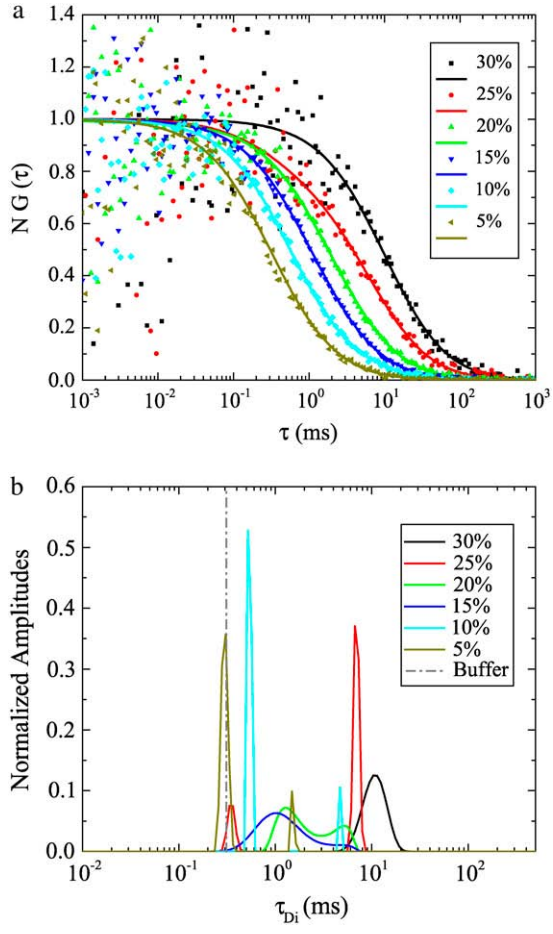

FIGURE 4 Diffusion of eGFP-CaM in solutions of 500 kDa dextran at different concentrations. (*a*) Semilog plot showing raw FCS data and the fits obtained using MEMFCS. (*b*) The corresponding normalized amplitude distributions obtained from the MEMFCS fit. Note that at 25% and 20% dextran solution, the amplitude splits into two components; for 20% the separation is more obvious by the broadened components.

of 500 kDa dextran (30%), the fits obtained from the MEMFCS show a broad distribution with relatively low amplitude reaching a maximum at $\tau_{DMax} = 10.38$ ms. The distribution sharpens at 25% dextran where a second component also appears at $\tau_{Di} \sim 0.3$ ms. This behavior is reminiscent of that observed for the 10 kDa dextran-TMR molecules in sol-gels. However, transitions in behavior start taking place at a concentration of 20% and 15% dextrans with similar distributions of τ_{Di}s showing two components that are close together. In the case of 10% dextrans, two diffusive mechanisms are evident, but the relative magnitudes of the two distributions are inverted, and now the highest amplitude corresponds to the peak at lower τ_{Di}s. A peak at higher τ_{Di}s with lower amplitude would correspond to a subdiffusive behavior where the eGFP-CaM were transiently trapped or hindered by the motion of the dextrans obstacles. At 5% dextrans, a similar pattern emerges, but the peak of both components is shifted to the left, indicating that both components are diffusing faster. Only a single diffusing component is evident when MEMFCS is applied to FCS measurements of eGFP-CaM when no dextran is present, (data not shown for clarity), and the peak falls very close to the faster diffusing component in the 5% trace.

Clearly MEMFCS is distinguishing two populations of eGFP-CaM diffusing in 500 kDa dextran. Furthermore, this method shows that at ~20% dextrans there is a transition between the dominant diffusive mechanisms. We interpret these data by assuming that nonrandom rearrangement occurs in the crowded dextran environment that produces two unique translational mobilities of eGFP-CaM. Physically, a plausible explanation is that the extended rod shape of the high molecular mass dextran permits the formation of transient structures that permit both less-hindered and more-hindered mobility of eGFP-CaM depending on the obstacle concentration. For the highest dextran concentration (30%), the probability of these structures forming is reduced, explaining why we observe only a single broad peak in the MEMFCS fits where the diffusive mechanisms can be ascribed only to the drag force felt by the molecule. At concentrations between 20% and 15%, some transition occurs where the 500 kDa dextran molecules attain some sort of ordered structure and the diffusive molecules sense different mechanism of diffusion. Table 2 summarizes the dextran data when it is clear that the subdiffusive exponent α loses the ability to distinguish the multiple components revealed by the MEMFCS fitting routine.

TABLE 2 Anomalous exponent for different concentrations of eGFP-CaM in 500 kDa dextran solution and compared to the fitting obtained using a multi-component model

500 kDa	30%	25%	20%	15%	10%	5%	0%
α	1	0.98	0.96	0.95	1	1	1
τ_a (ms)	10.58	5.6	2.20	1.29	0.8	0.42	0.31
τ_{DMax} (ms)	10.38	6.68 0.334	1.25 5.13	1.05 4.7	0.51 4.7	0.31 1.49	0.33

When two different diffusive mechanisms are observed, the first reported value is the one with highest amplitude and the second one is with the lowest peak amplitude.

DISCUSSION

MPFCS has been established as a sensitive and reproducible method to study diffusion both in vitro and in cells. Less well-established are appropriate models with which to analyze such data to derive biologically informative conclusions. Most often, it has been observed that a single component fit using Eq. 2 has failed to fully describe the details in the autocorrelation data measured in complex environments, and a more general form (Eq. 7) has been used to describe the experimental results (24–26). This model of anomalous diffusion describes the mean-square displacement of a molecule as being proportional to a power function of time. The exponent α describes this nonlinear behavior. When α is <1, the behavior is described as subdiffusion, and when α is >1, the behavior is superdiffusive. A number of investigators have applied the model of anomalous diffusion to describe their data (23,25–29). Some find clear evidence of subdiffusion, whereas others fail to find evidence for such behavior (27). Some of the studies of anomalous diffusion have been performed in protein suspensions (23), molecular crowding environments (24,25,27), and membrane proteins in heterogeneous lipid bilayers (28,30). Binding has also been reported to generate anomalous diffusion (31). However, it is worth mentioning that the anomalous diffusion model as represented by Eq. 7 may not accurately capture these underlying mechanisms. This is due to the fact that Eq. 7 is based on a propagator that satisfies a modified diffusion equation with a time-dependent diffusion coefficient. This time-dependent diffusion coefficient diverges on short timescales; therefore, the mathematical validity of Eq. 7 is unclear (25), limiting its utility in interpreting data from a biological perspective.

An additional approach for analyzing complex translational diffusion data is the maximum entropy method (3,20, 23,32). Periasamy and Verkman (32) adopted this approach to analyze both modeled and experimental fluorescence recovery after photobleaching data. They found that MEM was capable of distinguishing multiple-sized fluorescent species and was also useful at revealing underlying mechanisms of sub- and superdiffusion as defined using anomalous diffusion models. Sengupta et al. (3) developed a MEM fitting routine for FCS data and demonstrated its utility in distinguishing differences in the translational mobility of different-sized fluorescent tracers. Importantly, MEMFCS was found to be superior to conventional fitting routines, and its application to resolving species in heterogeneous environments was emphasized. We found that by applying the MEMFCS fitting routine to FCS data that were collected in both sol-gels and in dextran-crowded solutions, a number of important features in diffusional properties were revealed.

This was not the case when the same data were analyzed by the anomalous diffusion model (Eq. 7). A general conclusion that can be drawn from the data is that the anomalous diffusion model revealed only evidence of subdiffusion, while in some instances the MEMFCS fitting routine provided evidence of distinctly different diffusive mechanisms as discussed below.

Sol-gels provide a useful model system to study the impact of immobile barriers on translational diffusion when fully polymerized. Other groups have analyzed diffusion in sol-gels (33–35) when fully polymerized, and routinely concluded that the introduction of multi-component models was required to correctly fit the data. However, application of more sophisticated models was not applied in those studies. We took advantage of the time-dependence of our reaction to examine how fluorescent dextran molecules of increasing size diffuse as the sol-gel polymerizes. The diffusion of all four dextran-TMRs, 3 kDa, 10 kDa, 40 kDa, and 70 kDa within the sol-gel at time zero is significantly slowed relative to measurements in buffer (Table 1). In all cases except for the 70 kDa dextran (discussed below), there was evidence of subdiffusion when the data were analyzed with the anomalous model for at least one of the time points. When the data were analyzed with the MEMFCS fitting routine, two behaviors were revealed. One was that MEMFCS showed in all dextran sizes evidence of two maxima in the data for at least one of the time points studied. We conclude that first, the diffusing particles are sensing two fundamentally different environments, and such behavior from experimental (non-simulated) data has not been previously described in the literature. Second, there was significant broadening of the peaks most obvious in the 3 kDa and 10 kDa dextran data at certain time points. This behavior is consistent with that reported previously by Periasamy and Verkman (3), and Fradin and Banks (23), who both evaluated fluorescence recovery after photobleaching data and FCS data, respectively, with MEM routines. Both groups provided evidence of peak broadening in their data under environmental circumstances predicted to provide anomalous behavior. The data from the 70 kDa dextran at time zero revealed a sharp peak when analyzed by MEMFCS and concordantly showed an α-value of 1 when analyzed with the anomalous model. This was different than the broadened or multiple peaks evident with the 3 kDa, 10 kDa, or 40 kDa dextrans. We conclude that the size and shape of the tracer molecule in relation to the size of the crowding agent (sol-gel in this case) determines the translational diffusion distribution as reported by the MEMFCS, and this distribution is not due to artifactual factors since all of the experiments were accomplished under the same experimental conditions. The radius of the spherical sol particles at time zero would be < 50 nm, and it appears that the 70 kDa dextran (radius of gyration $\sim$8 nm) is large enough to avoid the appearance of multiple diffusive environments sensed by the smaller dextrans. When the sol-gel is no longer as dynamic, after 1 day, they behave as immobile barriers creating different pore sizes and complex wall structures. For large molecules, the pores serve as traps, but for smaller molecules the data show a clear evidence of subdiffusion, either by broadening of the amplitude distribution, as a signature of the heterogeneity in the sol-gel matrix, or for the decrease in the exponent α.

Molecular crowding, on the other hand, has been described with the volume exclusion principle introduced by Minton (36,37). A diagram of this idea is presented in Fig. 5, from which one can visualize how diffusion is obstructed by a molecule's ability to move in the presence of a crowding agent. This cartoon model captures a hypothetical physical description that encompasses the types of behavior we detected when analyzing the mobility of eGFP-CaM diffusing in various concentrations of 500 kDa dextran. In this case (disregarding polydispersity), the 500 kDa dextran behaves as a typical linear polymer finding a completely entangled regime at $>$10–15% (W. Pan and P. Vekilov, University of Houston, personal communication, 2006). At such regimes, one would expect multiple length scales with pores of different sizes. Thus, the crowding agent's relative spatial distribution in solution can adopt different arrangements as shown in Fig. 5. When smaller diffusive molecules (eGFP-CaM in our specific case) are moving through this environment, spatial heterogeneities are revealed. Importantly, this behavior would have been entirely overlooked had we relied on an anomalous model alone to evaluate the data. The results

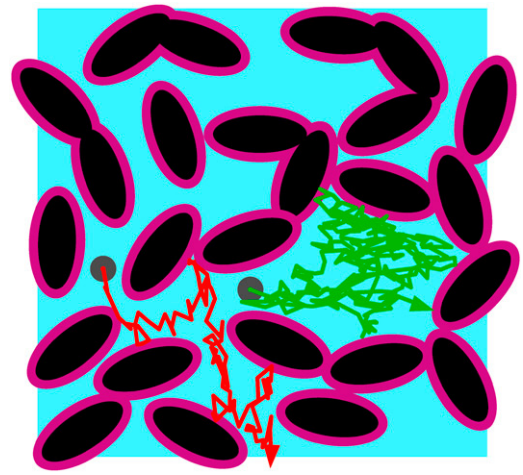

FIGURE 5 Cartoon description of how molecules could diffuse in a crowded environment. The volume exclusion principle restricts the spaces in which tracer molecules can diffuse (37). Our crowding agent is similar to a linear polymer with entangled regions. The center of a diffusive molecule can only find a place in the empty regions due to the physical restrictions of the dimensions of the obstacles (*black*) and the radius of the diffusive molecule (*gray*). In this particular example representing a highly heterogeneous environment, a molecule can diffuse less hindered in certain regions than others. Some structures could even cage the molecules for some period of time, producing a longer translational diffusion. At other regions, molecules appear to move freely as shown by traveling longer distances in the same period of time.

shown in Table 2 reveal that at all concentrations of 500 kDa dextran, there was no clear evidence of anomalous diffusion (α-value very close to or equal to 1). However, when analyzed with the MEMFCS fitting routine, evidence of multiple diffusive mechanisms was revealed. Two behaviors were simultaneously observed with the 25% concentration of 500 kDa dextran (Fig. 4). As suggested by some authors (38,39), a less-hindered component can be caused by the formation of secondary structures that reduce the level of anisotropy, allowing a molecule to diffuse faster in a particular direction, as illustrated in Fig. 5. The same principle will then apply for the case of subdiffusion where a molecule is transiently trapped or ''caged'', slowing its diffusion (see Fig. 5). Thus, MPFCS measurements of diffusion coupled with MEMFCS analysis have revealed potential underlying structural information within a heterogeneous environment.

CONCLUSIONS

We have used MEMFCS to analyze diffusion from a multicomponent point of view. Instead of using a power law exponent α as a way to quantify subdiffusion or superdiffusion, we have used the distribution of the amplitudes obtained by MEMFCS fit to describe the physical heterogeneity of the system. This continuous distribution of multiple components, applied to diffusion in heterogeneous nanostructures, revealed the existence of different mechanism of diffusion. However, when data were analyzed with an anomalous diffusion model (Eq. 7), only a subdiffusive mechanism was observed. When MEMFCS was applied to study of translational mobility in both sol-gels and in a crowding environment, we were able to distinguish multiple underlying mechanisms of diffusion, sometimes simultaneously, within one experimental condition.

Our data suggest the presence of different mechanisms of diffusion when a tagged molecule (dextran-TMR or eGFP-CaM) is placed in a heterogeneous environment like those used in our study. One is normal but slowed diffusion due to crowding, and can be characterized as Fickian diffusion. In some of our data, we observe a second component in the amplitude distribution. When the second component is faster than the principal peak, we conclude that the molecules have less-hindered mobility, in such a way that they exit the focal volume more quickly than the mean. This is due to the relative size between the tracer molecule and the dimensions of the crowding agent. In other occasions, the second peak is observed at slower characteristic times than the mean. For this particular case, we conclude that molecules have a subdiffusive-like behavior. This is consistent with the idea that the molecules can become transiently trapped in either mobile or immobile ''cages''. A signature of the heterogeneity in the environment is the fact that there is a clear correlation between the broadening of the amplitude distribution with the α-exponent in the anomalous diffusion model, suggesting a subdiffusive behavior. An important adjunct to our studies would be to apply numerical simulations of molecular diffusion in a well-defined crowded environment or with a prescribed jump/length/waiting time distribution and calculate the autocorrelation from it. From the simulated data, we will use MEMFCS and refine our understanding on whether anomalous diffusion gives rise to multiple components or vice versa. Along the same lines, it would be important to map the relative size of the diffusive molecule with respect to the dimensions of the mobile and immobile obstacles in which one could observe the multiple diffusive mechanisms. These efforts are under way.

In summary, our results support that MEMFCS methodology will be an important tool addressing translational mobility within the complex intracellular environment. We are currently applying MPFCS and MEMFCS to analyze the behavior of calmodulin and Ca^{2+}/calmodulin-dependent protein kinase II in the complex environment of the neuronal cytoplasm.

We thank Dr. Sudipta Maiti for kindly providing the MEMFCS software and Kanchan Garai for his supervision on using it. Also we thank Drs. Peter Vekilov and Vijay Iyer for fruitful discussions regarding this project and suggestions on this manuscript.

This work was supported by the Texas Advanced Research Program under Grant No. 011618 and the Human Frontier Science Program under Grant No. RGP0066.

REFERENCES

1. Zipfel, W. R., and W. W. Webb. 2001. In vivo diffusion measurements using multi-photon excited fluorescence photobleaching recovery and fluorescence correlation spectroscopy. *In* Methods in Cellular Imaging. A. Periasamy, editor. Oxford University Press, Oxford UK. 216–325.
2. Kim, S. A., K. G. Heinze, M. N. Waxham, and P. Schwille. 2004. Intracellular calmodulin availability accessed with two-photon cross-correlation. *Proc. Natl. Acad. Sci. USA.* 101:105–110.
3. Sengupta, P., K. Garai, J. Balaji, N. Periasamy, and S. Maiti. 2003. Measuring size distribution in highly heterogeneous systems with fluorescence correlation spectroscopy. *Biophys. J.* 84:1977–1984.
4. Kolb, S. J., A. Hudmon, T. R. Ginsberg, and M. N. Waxham. 1998. Identification of domains essential for the assembly of calcium/calmodulin-dependent protein kinase II holoenzymes. *J. Biol. Chem.* 273:31555–31564.
5. Putkey, J. A., and M. N. Waxham. 1996. A peptide model for calmodulin trapping by calcium/calmodulin-dependent protein kinase II. *J. Biol. Chem.* 271:29619–29623.
6. Vollet, D. R., D. A. Donatti, and A. Ibañez Ruiz. 1999. Hydrolysis rates of TMOS catalyzed by oxalic acid and stimulated by ultrasound. *J. Sol-Gel Sci. Tech.* 15:5–11.
7. Brinker, C. J., and G. W. Scherer. 1990. Sol-Gel Science: The Physics and Chemistry of Sol-Gel Processing. Academic Press, New York.
8. Ellerby, L. M., C. R. Nishida, F. Nishida, S. A. Yamanaka, B. Dunn, J. S. Valentine, and J. I. Zink. 1992. Encapsulation of proteins in transparent porous silicate glasses prepared by the sol-gel method. *Science.* 255:1113–1115.
9. Granath, K. A. 1958. Solution properties of branched dextrans. *J. Colloid Sci.* 13:308–328.
10. Larm, O., B. Lindberg, and S. Svensson. 1971. Studies on the length of the side chains of the dextran elaborated by Leuconostoc mesenteroides NRRL B-512. *Carbohydr. Res.* 20:39–48.
11. Iyer, V., M. Rossow, and M. N. Waxham. 2006. Peak two-photon molecular brightness of fluorophores is a robust measure of

quantum efficiency and photostability. *J. Opt. Soc. Am. B.* 23: 1420–1433.

12. Maiti, S., U. Haupts, and W. W. Webb. 1997. Fluorescence correlation spectroscopy: diagnostics for sparse molecules. *Proc. Natl. Acad. Sci. USA.* 94:11753–11757.
13. Berland, K., and G. Shen. 2003. Excitation saturation in two-photon fluorescence correlation spectroscopy. *Appl. Opt.* 42:5566–5576.
14. Nagy, A., J. Wu, and K. M. Berland. 2005. Observation volumes and {gamma}-factors in two-photon fluorescence fluctuation spectroscopy. *Biophys. J.* 89:2077–2090.
15. Mertz, J. 2003. Molecular photodynamics involved in multi-photon excitation fluorescence microscopy. *Eur. Phys. J. D.* 3:53–66.
16. Widengren, J., and R. Rigler. 2003. Mechanisms of photobleaching investigated by fluorescence correlation spectroscopy. *Bioimaging.* 4:l149–157.
17. Dittrich, P., and P. Schwille. 2001. Photobleaching and stabilization of fluorophores used for single-molecule analysis with one- and two-photon excitation. *Appl. Phys. B.* 73:829–837.
18. Meseth, U., T. Wohland, R. Rigler, and H. Vogel. 1999. Resolution of fluorescence correlation measurements. *Biophys. J.* 76:1619–1631.
19. Skilling, J., and R. K. Bryan. 1984. Maximum entropy image reconstruction: general algorithm. *Mon. Not. R. Astr. Soc.* 211:111–124.
20. Modos, K., R. Galantai, I. Bardos-Nagy, M. Wachsmuth, K. Toth, J. Fidy, and J. Langowski. 2004. Maximum-entropy decomposition of fluorescence correlation spectroscopy data: application to liposome-human serum albumin association. *Eur. Biophys. J.* 33:59–67.
21. Schwille, P., J. Korlach, and W. W. Webb. 1999. Fluorescence correlation spectroscopy with single-molecule sensitivity on cell and model membranes. *Cytometry.* 36:176–182.
22. Lan, E. H., B. Dunn, and J. I. Zink. 2005. Nanostructured systems for biological materials. *Methods Mol. Biol.* 300:53–79.
23. Banks, D. S., and C. Fradin. 2005. Anomalous diffusion of proteins due to molecular crowding. *Biophys. J.* 89:2960–2971.
24. Verkman, A. S. 2002. Solute and macromolecule diffusion in cellular aqueous compartments. *Trends Biochem. Sci.* 27:27–33.
25. Weiss, M., M. Elsner, F. Kartberg, and T. Nilsson. 2004. Anomalous subdiffusion is a measure for cytoplasmic crowding in living cells. *Biophys. J.* 87:3518–3524.
26. Weiss, M., H. Hashimoto, and T. Nilsson. 2003. Anomalous protein diffusion in living cells as seen by fluorescence correlation spectroscopy. *Biophys. J.* 84:4043–4052.
27. Dauty, E., and A. S. Verkman. 2004. Molecular crowding reduces to a similar extent the diffusion of small solutes and macromolecules: measurement by fluorescence correlation spectroscopy. *J. Mol. Recognit.* 17:441–447.
28. Ratto, T. V., and M. L. Longo. 2003. Anomalous subdiffusion in heterogeneous lipid bilayers. *Langmuir.* 19:1788–1793.
29. Schutz, G. J., H. Schindler, and T. Schmidt. 1997. Single-molecule microscopy on model membranes reveals anomalous diffusion. *Biophys. J.* 73:1073–1080.
30. Ratto, T. V., and M. L. Longo. 2002. Obstructed diffusion in phase-separated supported lipid bilayers: a combined atomic force microscopy and fluorescence recovery after photobleaching approach. *Biophys. J.* 83:3380–3392.
31. Saxton, M. J. 1996. Anomalous diffusion due to binding: a Monte Carlo study. *Biophys. J.* 70:1250–1262.
32. Periasamy, N., and A. S. Verkman. 1998. Analysis of fluorophore diffusion by continuous distributions of diffusion coefficients: application to photobleaching measurements of multicomponent and anomalous diffusion. *Biophys. J.* 75:557–567.
33. Mahurin, S. M., S. Dai, and M. D. Barnes. 2003. Probing the diffusion of a dilute dye solution in mesoporous glass with fluorescence correlation spectroscopy. *J. Phys. Chem. B.* 107:13336–13340.
34. Martin-Brown, S. A., Y. Fu, G. Saroja, M. M. Collinson, and D. A. Higgins. 2005. Single-molecule studies of diffusion by oligomer-bound dyes in organically modified sol-gel-derived silicate films. *Anal. Chem.* 77:486–494.
35. McCain, K. S., P. Schluesche, and J. M. Harris. 2004. Poly(amidoamine) dendrimers as nanoscale probes in Sol-Gel films investigated by total internal reflection fluorescence spectroscopy. *Anal. Chem.* 76: 939–946.
36. Minton, A. P. 2001. Effects of excluded surface area and adsorbate clustering on surface adsorption of proteins. II. Kinetic models. *Biophys. J.* 80:1641–1648.
37. Minton, A. P. 2001. The influence of macromolecular crowding and macromolecular confinement on biochemical reactions in physiological media. *J. Biol. Chem.* 276:10577–10580.
38. Nicholson, C., and E. Sykova. 1998. Extracellular space structure revealed by diffusion analysis. *Trends Neurosci.* 21:207–215.
39. Sykova, E. 2005. Glia and volume transmission during physiological and pathological states. *J. Neural Transm.* 112:137–147.